SPE-212592-MS

Permeability Prediction of Carbonate Cores With Gaussian Process Regression Model

Xingang Bu, Beijing Research Center, Aramco Asia; Hassan Saleh, Ming Han, and Abdulkareem AlSofi, EXPEC Advanced Research Center, Saudi Aramco

 DOI 10.2118/212592-MS

This paper was prepared for presentation at the SPE Reservoir Characterisation and Simulation Conference and Exhibition held in Abu Dhabi, UAE, 24 - 26 January 2023.

Abstract

Machine leaning (ML) methods are widely adopted in predictions affected by various factors. This paper presents a step-by-step workflow of applying a ML approach to develop a heterogeneous permeability prediction model from the CT images of core samples. In this work, over ten thousand 3-D sub-image were randomly extracted from the CT images of two heterogeneous carbonate core samples. The permeability of each sub-image is simulated using pore network modeling (PNM) method. Ten features including porosity, pore size, surface area, specific surface area and connection coefficient etc. are extracted from sub-image by a statistical method. Three training datasets were built with features and permeability. Each set of training data is input into a ML model pool, which contains 19 regression models of 5 types including linear regression models, regression trees, support vector machines, Gaussian process regression models and ensembles of trees. Then, regression models are trained to identify the one that can yield the best permeability prediction. The trained model with the highest R-Squared value is selected for permeability prediction from binary CT images. Overall, comparing the training outputs indicate that Gaussian Process Regression models (GPR) correlate features and permeability well. For the tested heterogeneous core plugs, the exponential Gaussian Process model performs the best. The R-Squared values of the three sets of training data are 0.88, 0.87 and 0.91 respectively. Afterwards, the selected ML model was tested with additional data, and the R-squared value of each test dataset was greater than 0.85, confirming a strong predictive performance. The trained model based on ML method eliminates the conventional time-consuming operations including distance transformation and watershed segmentation. It also avoids excessive memory consumption, which makes the method suitable for images with large size. The paper provides a way to develop an alternative approach of PNM simulation method for permeability prediction from CT images.

Introduction

Permeability is one of essential parameters for characterization of the rock property, and highly relevant to a wide range of application in petroleum engineering. It is dependent on the complex microstructure of

the rock pore space (Pape et al., 1999). Many studies showed that absolute permeability is closely related to petro-physical properties, such as porosity, pore geometry, pore size, connectivity, specific surface area, tortuosity and others (Carman 1956; Bear 1972, Katz and Thompson 1986; Sahimi 2011, Fu et al, 2021). However, there is no one analytical or empirical model that taking into account all these features to estimate the permeability of porous media accurately without solving for flow at the microscale. (Pan et al. 2001; Arns et al. 2004; Mostaghimi et al. 2013). Meanwhile, it is difficult to quantify some of these petro-physical properties.

Recently, the rapid development in digital rock physics (DRP) technology has been facilitated the characterization of microstructure features (Andra et al., 2013; Fu et al, 2011). The DRP technology applies advanced microscopy imaging facility (Blunt et al., 2013; Anovitz and Cole, 2015), such as X-ray computed tomography (CT), which is a nondestructive and noninvasive means to obtain 3-D geometries of pore microstructures (Hazlett, 1995; Lindquist et al., 1996; Wildenschild et al., 2013; Schluter et al., 2014). CT images currently can be obtained at resolution down to a few microns, which is sufficient to depict the pore space of conventional rocks (Flannery et al., 1987; Coenen et al., 2004). These images after processing are used for estimating rock properties with different methods.

Pore network modeling (PNM) and direct numerical simulation (DNS) are two primary methods to compute permeability at pore scale. PNM simplifies the complex pore space into a topologically representative network of pore bodies interconnected by pore throats with supposing shapes. The transport behaviors between pores and throats are described by semi-analytical laws (such as Hagen-Poiseuille law), which greatly reduces the computational cost and enables multi-scale modelling to incorporate heavy heterogeneity in large volumes. On the contrary, DNS directly discretizes the raw pore space into computing elements by preserving pore geometry (generally computing element is voxel), and then transport equations (such as Navier-Stokes or Laplace equations) are numerically solved or approximated on the computational meshes (Andrä et al., 2013; Blunt et al., 2013). Many methods such as finite difference method, finite element method, finite volume method, smoothed particle hydrodynamics method and Lattice Boltzmann method (LBM), are direct numerical simulation method. Generally, DNS can provide direct insight into the impact of pore microstructure on transport properties, but it is limited by computational intensity. The 3-D digital microstructure with large representative size and high resolution usually contains hundreds of millions of computational elements, which result in high computational cost (Liu et al., 2016; Saxena et al., 2017). Pore network modeling is preferred instead of more intensive direct numerical simulation since the simplified geometry makes it possible to efficiently simulate much larger 3-D digital rock volume (Moussa et al., 2021).

The advancement of artificial intelligence promotes researchers attempt to apply machine learning (ML) to estimate permeability, the method can reduce the computational costs significantly while maintaining the level of accuracy. Wu et al. (2018) predicted the permeability based on simple 2-D synthetic images with ML method. Sudakov et al. (2019) tested the applicability of predicting permeability with gradient boosting and deep neural networks. Araya-Polo et al (2020) estimated permeability of 2-D sections images from 11 clastic reservoirs using convolutional neural network (CNN). Rabbani et al. (2019) trained an Artificial Neural Network to simulate the trend of throat's permeability based on image-based features, and to reduce the overall computational cost. Kamrava et al. (2020) linked the morphology of porous media to their permeability using a deep learning algorithm. Moussa et al (2021) applied deep neural network and convolutional neural network to predict permeability from 3-D CT images. These research results indicate machine learning (ML) is a powerful method for permeability prediction from CT-images at low computation cost.

In this paper, sub-images were extracted from CT images to build dataset for training a series of machine and deep learning-based models. The objective is to find one model that can achieve comparable accuracy at low computation cost for predicting permeability of heterogeneous carbonate core plugs. The features of the sub-image is obtained by statistical method and the permeability of the sub-image is simulated using pore

network modeling method. The features and simulated permeability of each set are fed into a ML model pool to train different machine or deep learning models. Based on the four metrics, the Gaussian process regression model with exponential kernel performs yielded the best permeability prediction performance. Finally, we test the found model with additional test data, confirming a strong predictive performance.

Images processing and permeability simulation

Two carbonate samples were imaged for the workflow development. The diameter of the two cylindrical samples is 10 mm, and the length is also 10 mm. Each image is composed of about one thousands slices with a size of 1000×1024 voxels. The resolution of the slice is 10.53 um. Other properties are listed in Table 1. The images are segmented by threshold method, and the measured porosity is used as a benchmark for images segmentation. Fig.1 shows a sample image and the corresponding segmented binary image. It can be seen that the image captured more than 95% of the pores, and the method of threshold segmentation can effectively separate pores and rocks. The segmented images are input for pore network extraction and permeability simulation. The improved algorithm based on the open source toolkit of PoreSpy (Gostick, 2017; Gostick et al., 2019) is used for pore network extraction, and the open source toolkit of OpenPNM (Gostick, et al., 2016) is used for permeability simulation.

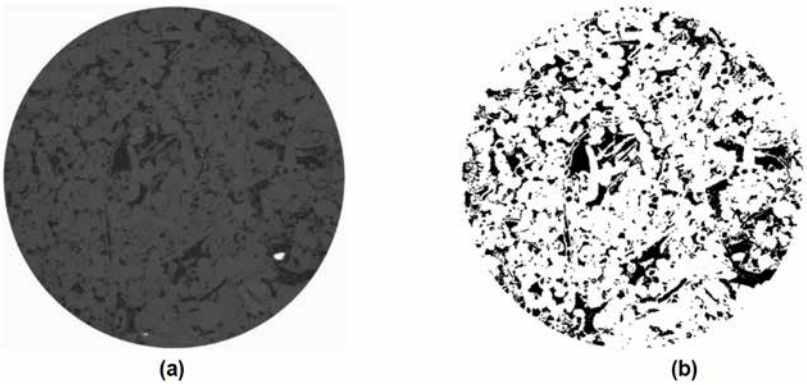

Figure. 1—A sample image and the corresponding binary image
(a) Greyscale image and (b) Binary image (black represents pores)

Table 1—Properties of samples and image information

No.	Size D×L, mm	Porosity, fraction	Permeability, mD	Image size, voxel
ImgA	10×10	0.214	719	1000×1024×916
ImgB	10×10	0.24	1050	1000×1024×819

PoreSpy and pore network model extraction

PoreSpy is a toolkit of Python package for quantitative analysis of porous media images, and used to extract pore network model. The binary images are operated with this toolkit, including distance transform, Gaussian smooth and marker-controlled watershed segmentation. After watershed segmentation, the pore voxels are labeled with an integer named marker for pore network model extraction. The pore space is approximated by a network of bonds (throats) and nodes (pores) with an idealized geometry. In our work, a ball represents the pore and a stick represents the throat. Pore location, volume, surface area and the connection information were measured and saved in the pore network.

Gaussian blur filter is used to smooth the image and remove or minimize the spurious pores (Gostick, 2017) in the algorithm of pore network extraction. The radius of the spherical structuring element and the standard deviation of the Gaussian distribution (Sigma) are two important parameters of Gaussian filter. In

order to catch the parameters that can achieve the best representation of the pore structure, the radius and Sigma of the filter were optimized by sensitivity study. The radius of the spherical Gaussian filter changes from 1 to 5 voxels, and the sigma ranges from 0.2 to 0.6. The parameters that minimizes the difference between the simulated and measured permeability are optimal. Sensitivity studies show that the permeability simulated with a radius of 3 and a Sigma of 0.4 can match the measured permeability well.

OpenPNM and permeability simulation

A toolkit of OpenPNM is used to simulate permeability, which is an open source package to provide a ready-made framework for performing pore network simulations of transport in porous materials (Gostick, et al., 2016). This toolkit is developed based on the pore network model (PNM), which describes the flow and the transport on the pore scale. The transport of fluid is simulated with Stokes flow in this study. The fluid velocity in the throat which compose the pore network is given by the Poiseuille parabolic profile. A constant pressure drop is specified across the network and to calculate the flow rate, then the permeability is determined based on Darcy's law. Details related to the PNM method can be found from published papers everywhere (Lenormand et al., 1983; Bakke et al., 1997; Christos et al., 2000; Varloteaux et al., 2013).

Data acquisition

In this work, regression method is used to develop permeability prediction model. Fig. 2 shows a workflow of data acquisition, which includes sub-image preparation, features extraction, pore network construction, permeability simulation and training data building. The input is the extracted binary sub-image. The workflow has two branches. The top branch uses the pore network model to simulate permeability, and the bottom branch extracts pore characteristics as features by a statistical analysis method. The simulated permeability and the extracted features are combined together as training input data. What needs to be emphasized here is the difference between pore segmentation and pore detection. Pore segmentation is to segment the connected pores into individual pores by watershed method, while pore detection is to detect the separated objects and the connected pores are considered as one pore.

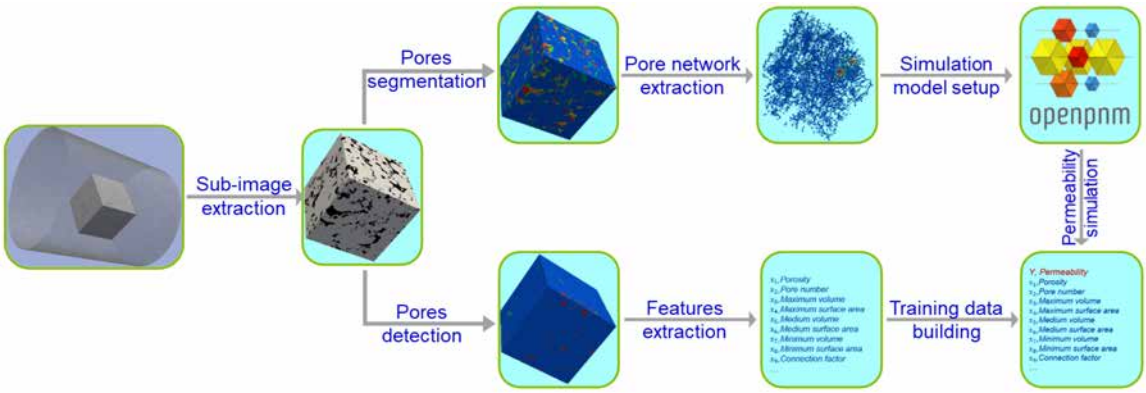

Figure. 2—Workflow of the training data building

Sub-image preparation

As mentioned previously, two carbonate samples were used to prepare the training dataset. To generate a dataset, the sub-image was randomly extracted from the original images. The sub-image consists of 300×300×300 voxels. One set of sub-image was extracted from each sample, respectively. 6002 sub-images were extracted from sample ImgA and 4568 sub-images were extracted from sample ImgB. Each of these sub-images can be considered as an independent rock image, and retaining some geometrical features of the parent sample.

Feature extraction

A binary sub-image is input to extract features, as shown in the bottom branch of Fig.2. Without operation of pores segmentation, voxels of connected pores in binary sub-image is considered as one pore. Thereby, this pore number is different from that counted from segmented pores, and much less than the later. We considered a number of network model features, which could influence the permeability for a given sample. These features are porosity, pore number, maximum pore volume, maximum surface area, mean pore volume, mean surface area, median pore volume, median surface area, minimum pore volume, minimum surface area, specific surface area and connection factor. The connection factor is defined as the ratio of the volume of the largest pore to the total pore volume.

Building ground truth data

The approach of pore-scale network modeling is used to compute permeability of sub-images in the dataset. The network model is a simplified representation of rock geometry, consisting of spherical pores connected by cylindrical throats. The network representation is then used to compute the permeability of each sub-image, making use of Darcy's law and taking the flow type to be Stokes flow.

As the top branch of the workflow presented in Fig.2, the connected pores of input binary sub-image are segmented using watershed segmentation algorithm. This algorithm uses Euclidean distance transform of binary objects to detect the narrowest parts of the connections between different nodes. The output of the watershed segmentation is an image with isolated segments each of which represents a unique pore body. More details on the methodology and validation of watershed segmentation algorithm can be found in papers (Rabbani et al., 2014; Gostick, 2017). The pore network model is created from the segmented sub-image using the improved PoreSpy toolkit and the previous optimized parameters. The generated pore network is fed into OpenPNM toolkit to simulate different physics and processes, and the simulation results are assumed to be the ground truth for training the permeability models.

Regression models

We apply regression methods to develop permeability prediction models that can reduce computational costs compared to the previously mentioned simulation methods. In this method, the sub-image is simplified to a vector (features) which represents the pores characteristic. With this way, the application of the trained model becomes fast and easy. 19 regression models of 5 types including linear regression models, regression trees, support vector machines, Gaussian process regression models and ensembles of trees, were put into a ML model pool for finding one that can yield the best permeability prediction performance.

Models training

Following the data acquisition process presented above, 3 sets of training data were built. The training dataset A and B contain 6002 and 4568 data pairs, respectively. The dataset A is generated from sample ImgA, and dataset B is generated from sample ImgB. The dataset AB contains 10570 data pairs, which is a combination of the dataset A and B. Each data pair contains a vector describing the pores characteristic of the sub-image, and a corresponding permeability that is simulated with pore network modeling approach. Each of dataset is fed into the model pool to find the model that can yield the best permeability prediction performance.

Results and discussion

Evaluation metrics and score

We trained all models using Matlab Regression Learner application. During training, four metrics are monitored to assess the model reliability: root mean square error (RMSE), coefficient of determination(R-Squared), mean squared error (MSE) and mean absolute error (MAE). RMSE measures the difference

between the values predicted by a model and the values observed. R-squared indicates the proportionate amount of variation in the response variable explained by the independent variables in the linear regression model. The larger the R-squared is, the more variability is explained by the linear regression model. RMSE and R-Squared are very common criteria for regression problem monitoring.

In this study, 5-fold cross-validation is used to estimate loss based on mean squared error. This approach split the observations and the response variable into 5 groups, each of which has approximately the same number of observations. Each group of the 5 groups will be acted as test data exactly once and rest groups are training data. The best model was determined by the score of RMSE, and R-Squared, MSE and MAE as additional standards. The score of the metrics are reported in the Table 2. The MAE is ignored due to the limitation of the table size, and which equal to the square of the RMSE. The training results of three datasets show the same trend. The permeability predicted using Gaussian process regression (GPR) models exhibited minimum RMSE and highest R-Squared. In this type of model, exponential GPR model shows the best performance. The R-Squared values of exponential GPR model are 0.88, 0.87 and 0.91 for three sets of training data. For convenience, we label the models trained from datasets A, B, and AB as Ma, Mb, and Mab, respectively.

Table 2—Performance of the different models

Model Type	Models	Dataset A			Dataset B			Dataset A+B		
		RMSE	R-Squared	MAE	RMSE	R-Squared	MAE	RMSE	R-Squared	MAE
Linear Regression Models	Linear	132.6	0.7	101.8	374.2	0.78	282.4	279.5	0.83	195.0
	Interactions Linear	119.9	0.75	91.2	342.6	0.82	252.4	254.1	0.86	172.4
	Robust Linear	133.3	0.69	101.1	376.4	0.78	280.4	293.2	0.82	189.8
	Stepwise Linear	121.6	0.74	92.9	338.0	0.82	249.0	251.9	0.86	172.0
	Average	**126.9**	**0.72**	**96.8**	**357.8**	**0.80**	**266.0**	**269.7**	**0.84**	**182.3**
Regression Trees	Fine Tree	113.2	0.78	80.3	384.7	0.77	276.4	263.0	0.85	163.2
	Medium Tree	110.6	0.79	80.2	359.0	0.8	259.0	251.6	0.87	159.4
	Coarse Tree	115.8	0.77	85.6	352.5	0.81	257.0	247.3	0.87	159.5
	Average	**113.2**	**0.78**	**82.1**	**365.4**	**0.79**	**264.1**	**253.9**	**0.86**	**160.7**
Support Vector Machines	Linear SVM	150.9	0.61	106.9	376.2	0.78	280.4	284.8	0.83	189.3
	Quadratic SVM	116.6	0.76	85.3	337.7	0.82	243.8	250.2	0.87	165.1
	Cubic SVM	108.1	0.8	78.7	321.4	0.84	232.4	491.2	0.49	275.2
	Fine Gaussian SVM	96.6	0.84	66.9	323.8	0.84	234.1	221.7	0.9	139.6
	Medium Gaussian SVM	105.1	0.81	76.5	318.8	0.84	228.1	237.9	0.88	154.4
	Coarse Gaussian SVM	127.6	0.72	94.4	358.9	0.8	259.7	263.5	0.85	174.0
	Average	**117.5**	**0.76**	**84.8**	**339.5**	**0.82**	**246.4**	**291.6**	**0.80**	**183.0**
Gaussian Process Regression Models	Rational Quadratic	82.7	0.88	58.7	293.3	0.87	210.9	209.7	0.91	130.4
	Squared Exponential	91.0	0.86	67.9	302.7	0.86	219.1	212.0	0.9	138.5
	Matern 5/2	87.2	0.87	64.7	295.5	0.87	213.0	206.9	0.91	134.7
	Exponential	81.4	0.89	57.6	289.3	0.87	208.6	205.4	0.91	126.9
	Average	**85.6**	**0.88**	**62.2**	**295.2**	**0.87**	**212.9**	**208.5**	**0.91**	**132.6**
Ensembles of Trees	Boosted Trees	115.4	0.77	85.0	336.7	0.83	243.7	246.5	0.87	162.4
	Bagged Trees	96.0	0.84	70.0	309.6	0.85	225.5	214.5	0.9	136.5
	Average	**105.7**	**0.81**	**77.5**	**323.1**	**0.84**	**234.6**	**230.5**	**0.89**	**149.4**

Gaussian Process Regression Model

A Gaussian process is a collection of random variables, any finite number of which have a joint Gaussian distribution. It is completely specified by its mean function *m(x)* and co-covariance function *k(x,x')* (Rasmussen, 2006). If $\{f(x), x_i \in R^d\}$ is a Gaussian process, then:

$$E(f(x)) = m(x) \tag{1}$$

$$Cov[f(x),\ f(x')] = E[\{f(x) - m(x)\}\{f(x') - m(x')\}] = k(x, x') \tag{2}$$

Consider the following model:

$$h(x)^T \beta + f(x) \tag{3}$$

where $f(x) \sim GP(0, k(x,x'))$, that is *f(x)* are from a zero mean GP with covariance function *k(x,x')*. *h(x)* are a set of basis functions that transform the original feature vector x in R^d into a new feature vector *h(x)* in R^p, β is a p -by-1 vector of basis function coefficients. This model represents a GPR model. An instance of response y can be modeled as

$$P(y_i | f(x_i),\ x_i) \sim N(y_i | h(x_i)^T \beta + f(x_i),\ \sigma^2) \tag{4}$$

Hence, a GPR model is a probabilistic model. There is a latent variable $f(x_i)$ introduced for each observation x_i, which makes the GPR model nonparametric (Matlab, 2020b). Training a GPR model is to estimate the basis function coefficients, β, the noise variance, σ^2, and the hyperparameters, θ, of thkernel function from the data.

For supervised learning, which is expected that the points with similar predictor values x_i, and naturally have close response valuesy_i. In Gaussian processes, the covariance function expresses this similarity (Rasmussen, 2006), and can be defined by kernel function. In this study, we found that Gaussian process model with exponential kernel performs best for the tested heterogeneous core plugs. The exponential kernel function is defined by:

$$k(x_i, x_j | \theta) = \sigma_f 2 \exp\left(-\frac{r}{\sigma_l}\right) \tag{5}$$

where σ_f is the signal standard deviation, σ_l is the characteristic length scale, and

$$r = \sqrt{(x_i - x_j)^T (x_i - x_j)} \tag{6}$$

Model performance

Previously, we presented the scores of different models, which indicates that the Gaussian process model with exponential kernel shows best performance. Fig. 3 shows the comparison of the prediction and observation of the three training datasets. It can be seen that the prediction results of three datasets show similar trends. The R-squared of model Mab is higher than that of Ma and Mb, which indicate that the training data has an important impact on the model. The permeability of training data in a wider range can generate a model with powerful predictive capability. The RMSE value of Mb is 295.2, which is higher than that of Ma of 85.6. This obvious difference is due to the difference in permeability and heterogeneity of the samples. The permeability of sample ImgB and ImgA is 1014 mD and 787 mD, respectively. It seems that the difference in permeability is not very obvious, but the range of permeability of the training data is very different. The maximum permeability of the dataset A is about 1600 mD, but it is about 4000 mD for dataset B. This difference also affects the RMSE value of model Mab, which is between model Ma and Mb.

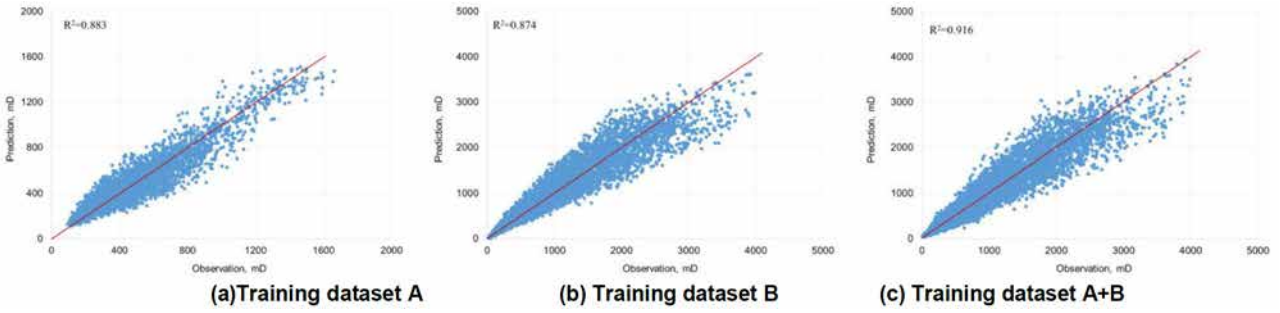

Figure.3—Prediction of permeability using exponential GP model

Figs. 4 to 6 show the correlation between the predicted permeability and extracted features from the training images of three datasets. These features include (a) porosity, (b) specific surface area, (c) connection coefficient, (d) maximum pore volume, (e) average pore size, and (f) average surface area. In this study, the connected pores are not segmented into individual pores in order to save computation time. Most of the pores discussed here are composed of many interconnected pores, and only a small part is isolated unconnected pores. Thereby, the individual pore volume here is somewhat different from the general concept of pore volume. The connection coefficient is the ratio of the maximum pore volume to the total pore volume. Checking the correlation between these features and permeability, we can see that some features show strong correlation with permeability, such as porosity, maximum pore volume, and connection coefficient, while other features show weak correlation. Examining the correlations found that a linear relationship is difficult to describe the relationship between features and permeability. From figures 4(a), 5(e) and (f), 6(e) and 6(f), it can be seen that the permeability varies widely for the features with the same value, and the distribution of data points exhibits cluster characteristics. These findings demonstrate the diversity of pore structure and the heavy heterogeneity of permeability.

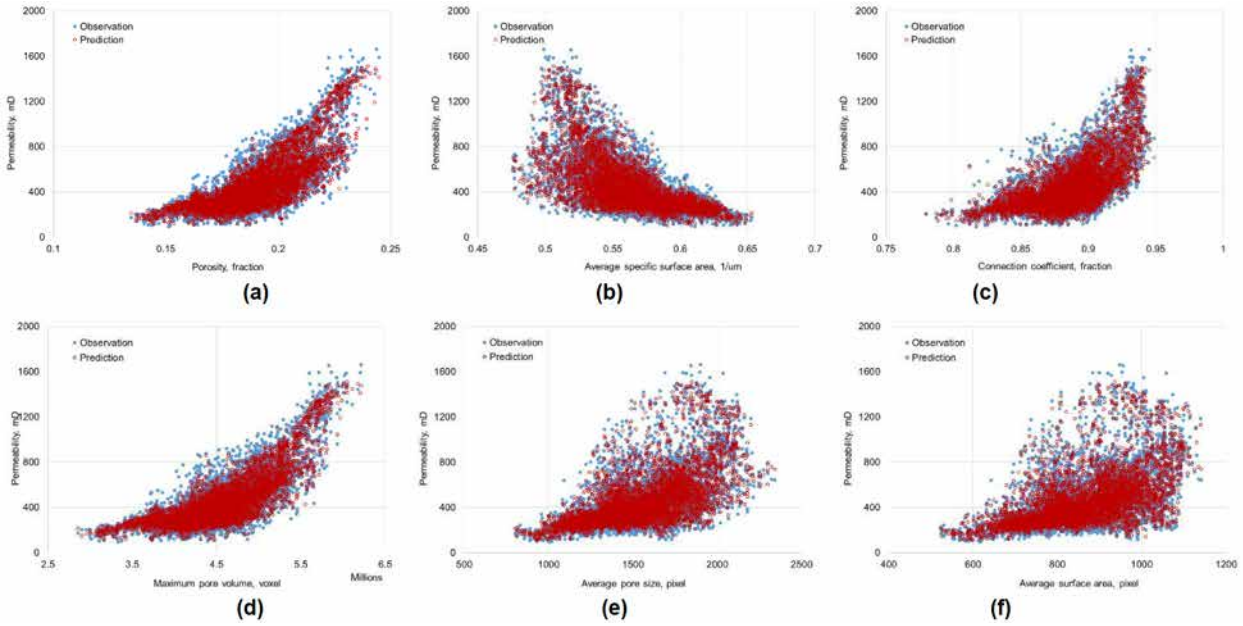

Figure.4—Scatter plot of predicted permeability vs. values of 6 extracted features of training dataset A (a) porosity, (b) specific surface area, (c) connection coefficient, (d) maximum pore volume, (e) average pore size, and (f) average surface area

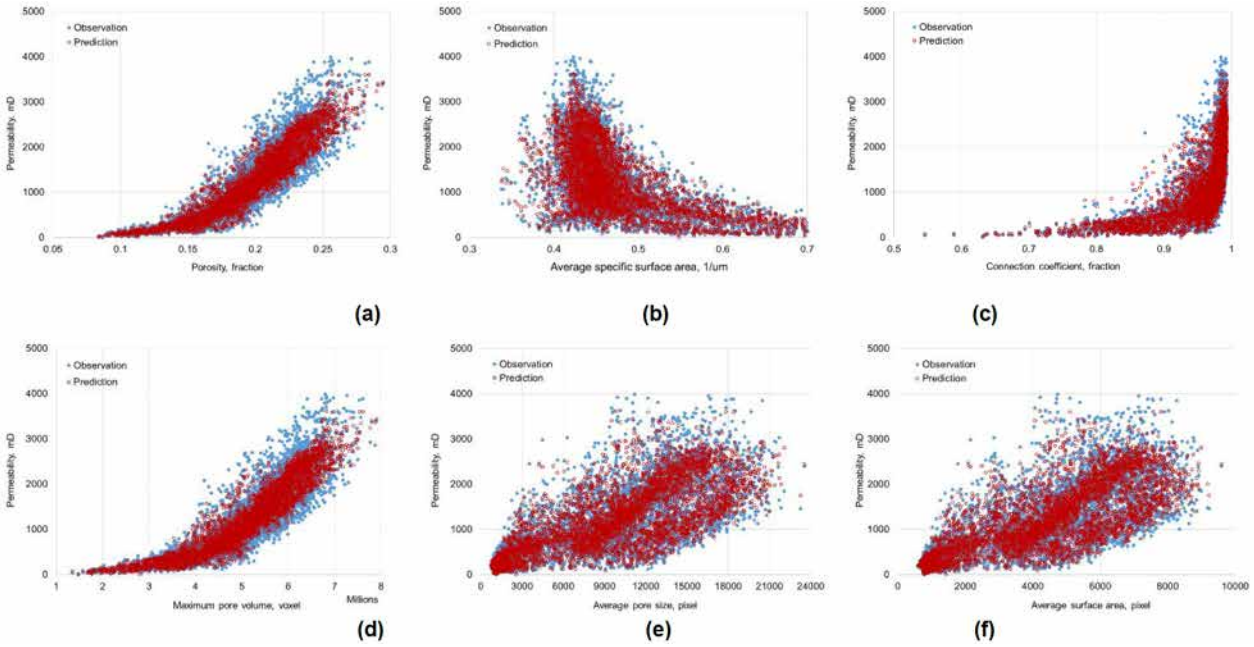

Figure.5—Scatter plot of predicted permeability vs. values of 6 extracted features of training dataset B (a) porosity, (b) specific surface area, (c) connection coefficient, (d) maximum pore volume, (e) average pore size, and (f) average surface area

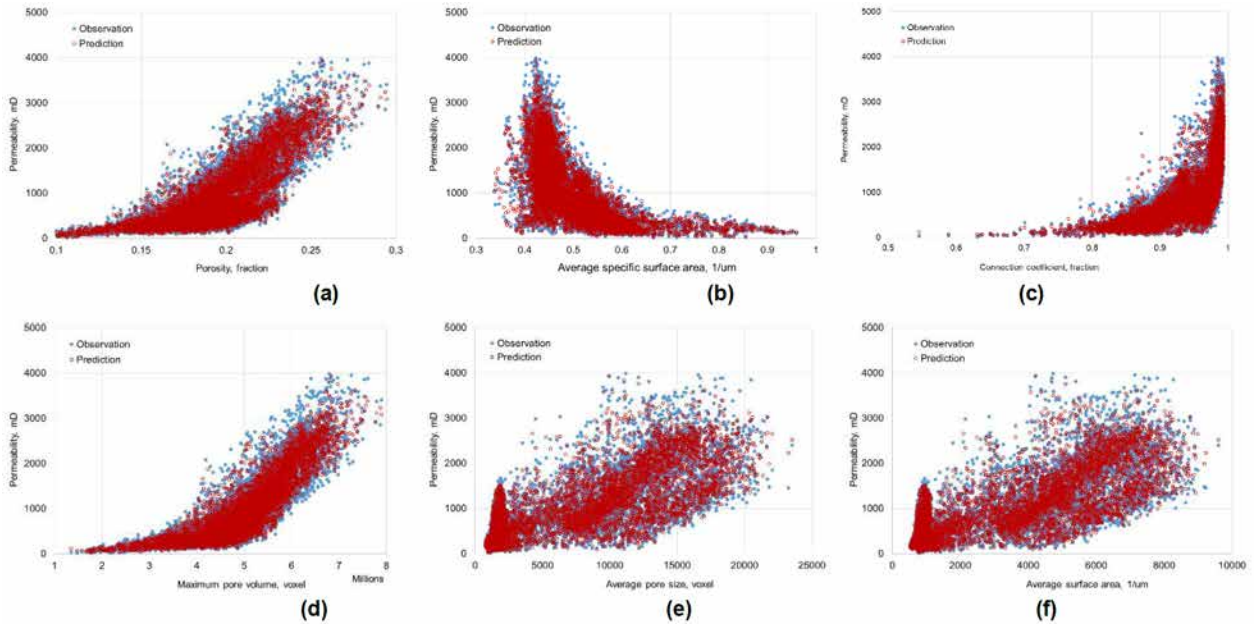

Figure.6—Scatter plot of predicted permeability vs. values of 6 extracted features of training dataset AB (a) porosity, (b) specific surface area, (c) connection coefficient, (d) maximum pore volume, (e) average pore size, and (f) average surface area

Permeability prediction

In order to test the reliability of the trained models for permeability prediction. Two sets of sub-images Tsa and Tsb were extracted from the original core image ImgA and ImgB, respectively. The size of sub-image is same as that of the training data used previously. The permeability of set Tsa and Tsb are predicted with the models Ma and Mb, respectively. Meanwhile, the model Mab are also used to predict the permeability of set Tsa and Tsb. Fig. 7 shows the permeability of the test data Tsa predicted with the models Ma and Mab respectively. The R-squared value of predictions are 0.929 and 0.933, which show better predicted results. Fig.8 presents the prediction results of Tsb predicted with models Mb and Mab, and the R-squared value

of predictions are 0.859 and 0.857. For each of set of test data, the prediction results of the two models are very similar. The prediction results of test data Tsa is a little better than that of test data Tsb according to the R-squared values. In Fig.8, it can be seen that the high permeability values (3000-4000 mD) of prediction significantly deviated from the observations. Recalling Figs. 3(b) and (c), it can be found that the training data points are relatively few in the range of 3000-4000mD, which may lead to a weaker prediction ability of the trained model for this range of data.

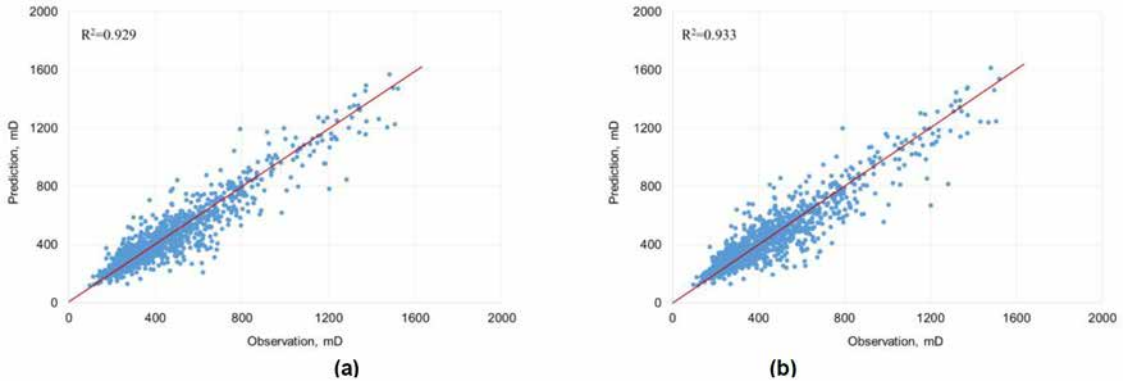

Figure.7—Prediction of permeability using trained models (a) trained using dataset A, (b) trained using dataset AB

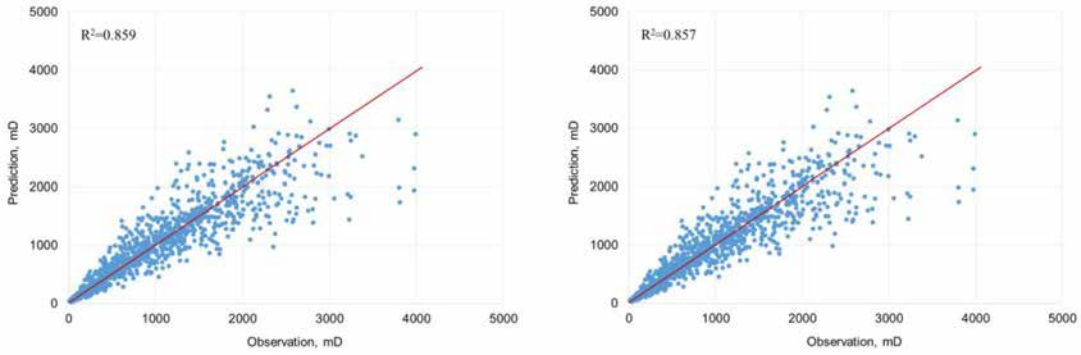

Figure.8—Prediction of permeability using trained models (a) trained using dataset B, (b) trained using dataset AB

Conclusions

In this study, we extracted sub-images from CT images to build training datasets for finding one machine or deep learning-based model to predict permeability form CT images. In this regards, 3 datasets were built and 19 regression models were trained. The main conclusions are as follow:

1. Machine learning based regression modeling can be an alternative approach of PNM simulation method for permeability prediction from CT images.
2. The exponential Gaussian Process Regression model show best performance among 19 models for the targeted CT images.
3. The training data has a significant impact on training the model, and a wider range of training data can generate a model with better predictive capability.
4. The correlation between features and permeability indicates the diversity of pore structure and the heterogeneity of permeability.

References

Andrä H. Combaret N., Dvorkin J., Glatt E., Han J., Kabel M., Keehm Y., Krzikalla F., Lee M., Madonna C., Marsh M.,(2013). Digital rock physics benchmarks—part II: Computing effective properties,Computers & Geosciences,**50**: 33–43,https://doi.org/10.1016/j.cageo.2012.09.008.

Anovitz, L. M. and Cole, D. R. (2015). Characterization and analysis of porosity and pore structures. *Reviews in Mineralogy and Geochemistry*, **80**(1):61–164.

Araya-Polo, M., Alpak, F.O., Hunter, S., et al (2020). Deep learning–driven permeability estimation from 2D images. *Comput Geosci* **24**, 571–580. https://doi.org/10.1007/s10596-019-09886-9

Arns, C. H., Knackstedt, M. A., Pinczewski, V. W., et al (2004). Virtual Permeametry on Microtomographic Images. *J Pet Sci Eng* **45** (1–2): 41–46.https://doi.org/10.1016/j.petrol.2004.05.001.

Bakke, S., and Pål-Eric, Ø..(1997). "3-D Pore-Scale Modelling of Sandstones and Flow Simulations in the Pore Networks." *SPE J*. **2**: 136–149. doi: https://doi.org/10.2118/35479-PA

Bear, J. (1972). Dynamics of Fluids in Porous Media. Mineola, New York, USA: Dover Publications.

Blunt M. J., Bijeljic B., Dong H., Gharbi, O. Iglauer, S., Mostaghimi, P., Paluszny, A., Pentland, C. (2012). Pore-scale imaging and modelling, *Advances in Water Resources* **51** (2013) 197–216. Doi: 10.1016/j.advwatres.03.003.

Carman, P. C. (1956). Flow of Gases through Porous Media. Waltham, Massachusetts, USA: Academic Press Inc.

Christos D. Tsakiroglou, Alkiviades C. Payatakes, (2000) Characterization of the pore structure of reservoir rocks with the aid of serial sectioning analysis, mercury porosimetry and network simulation, *Advances in Water Resources*, Volume **23**, Issue 7, Pages 773–789, https://doi.org/10.1016/S0309-1708(00)00002-6.

Coenen, J. G. C. and Xu Jing. (2004). "Measurement Parameters and Resolution Aspects of Micro X-Ray Tomography for Advanced Core Analysis."

Fu, J.L., Li, D.F., Thomas, H., and Li, C.F. (2021). Permeability prediction for natural porous rocks through feature selection and machine learning. 10.13140/RG.2.2.31190.78403.

Flannery B. P. Deckman H. W. Roberge W. G., et al 1987. Three-Dimensional X-Ray Microtomography. *Science* **237** (4821): 1439–1444. DOI: 10.1126/science.237.4821.1439

Hieu, D.N., Minh, T.T, Quang, T.V., et al (2016). Machine Learning-Based Approach for Predicting the Execution Time of CFD Applications on Cloud Computing Environment, *in: International Conference on Future Data and Security Engineering*, pp. 40–52.

Itu, L., Rapaka, S., T. Passerini, T., Georgescu, B., Schwemmer, C., Schoe, M., Binger, S., Flohr, T., Sharma, P., Comaniciu, D. (2016) A machine-learning approach for computation of fractional ow reserve from coronary computed tomography, *Journal of Applied Physiology* **121** (1) :42–52.

Gostick J, Khan ZA, Tranter TG, Kok MDR, Agnaou M, Sadeghi MA, Jervis R. (2016) .PoreSpy: A Python Toolkit for Quantitative Analysis of Porous Media Images. *Journal of Open Source Software*, 2019. doi:10.21105/joss.01296

Gostick, J.T., (2017). Versatile and efficient pore network extraction method using marker-based watershed segmentation. *PHYSICAL REVIEW E*, **96**(2), 023307.

Gostick J, Aghighi M, Hinebaugh J, Tranter T, Hoeh MA, Day H, Spellacy B, Sharqawy MH, Bazylak A, Burns A, Lehnert W. (2016). OpenPNM: a pore network modeling package. *Computing in Science & Engineering*. May 25; **18**(4):60–74. doi:10.1109/MCSE.2016.49.

Moussa Tembely, M., AlSumaiti, A.M., .Alameri, W.S. (2021). Machine and deep learning for estimating the permeability of complex carbonate rock from X-ray micro-computed tomography, *Energy Reports*, **7**, 1460–1472

Lenormand, R., Zarcone, C., & Sarr, A. (1983). Mechanisms of the displacement of one fluid by another in a network of capillary ducts. *Journal of Fluid Mechanics*, **135**, 337–353. doi:10.1017/S0022112083003110

Liu, J., Pereira, G. G., Liu, Q., and Regenauer-Lieb, K. (2016). Computational challenges in the analyses of petrophysics using microtomography and upscaling: a review. *Computers & Geosciences*, **89**:107–117.

Matlab documentation R 2020b,

Mostaghimi, P., Blunt, M. J., and Bijeljic, B. (2013). Computations of Absolute Permeability on Micro-CT Images. *Math Geosci* **45** (1): 103–125. https://doi.org/10.1007/s11004-012-9431-4.

Kamrava, Serveh & Tahmasebi, Pejman & Sahimi, Muhammad. (2020). Linking Morphology of Porous Media to Their Macroscopic Permeability by Deep Learning. *Transport in Porous Media*. **131**. 10.1007/s11242-019-01352-5.

Katz, A. J. and Thompson, A. H. 1986. Quantitative Prediction of Permeability in Porous Rock. *Phys Rev B* **34** (11): 8179–8181. https://doi.org/10.1103/PhysRevB.34.8179.

Qingrong X., Baychev, T.G., Jivkov, A. P. (2016),. Reviewof pore network modelling of porous media: Experimental characterizations, network constructions and applications to reactive transport, *Journal of Contaminant Hydrology*, https://doi.org/10.1016/j.jconhyd.2016.07.002.

Pan, C., Hilpert, M., and Miller, C. T. (2001). Pore-Scale Modeling of Saturated Permeabilities in Random Sphere Packings. *Phys Rev E* **64** (6): 066702. https://doi.org/10.1103/PhysRevE.64.066702.

Pape, H., Clauser, C., and Iffland, J. 1999. Permeability prediction based on fractal pore-space geometry. *Geophysics* **64**(5): 1447–1460. https://doi.org/10.1190/1.1444649

Rabbani, A., Babaei, M., Shams, R., Wang, Y.D., Chung, T. (2020). DeePore: A deep learning workflow for rapid and comprehensive characterization of porous materials, *Advances in Water Resources*, **Volume 146**, https://doi.org/10.1016/j.advwatres.2020.103787.

Rabbani A., Saeid Jamshidi, Saeed Salehi, An automated simple algorithm for realistic pore network extraction from micro-tomography images, *Petrol J. Sci. Eng*. (2014), https://doi.org/10.1016/j.petrol.2014.08.020.

Sahimi, M. (2011). Flow and Transport in Porous Media and Fractured Rock: From Classical Methods to Modern Approaches, second edition, New York City, New York, USA: Wiley.

Saxena, N., Hofmann, R., Alpak, F. O., Berg, S., Dietderich, J., Agarwal, U., Tandon, K., Hunter, S., Freeman, J., and Wilson, O. B. (2017). References and benchmarks for pore-scale flow simulated using micro-ct images of porous media and digital rocks. *Advances in Water Resources*, **109**:211–235.

Van Der Linden, J. H., Narsilio, G. A., Tordesillas, A. (2016). Machine learning framework for analysis of transport through complex networks in porous, granular media: A focus on permeability, *Physical Review E* **94** (2). doi:10.1103/PhysRevE.94.022904.

Varloteaux C., Vu M.T., Békri S., Adler P.M. (2013). Reactive transport in porous media: pore-network model approach compared to pore-scale model. *Phys Rev E Stat Nonlin Soft Matter Phys. Feb*;**87**(2):023010. doi:10.1103/PhysRevE.87.023010. Epub 2013 Feb 15. PMID: 23496613.

Wu, J., Yin, X., Xiao, H., (2018). Seeing permeability from images: fast prediction with convolutional neural networks. *Sci. Bull*. **63**(18), 1215–1222. https://doi.org/10.1016/j.scib.2018.08.006